JPE 16-6-18

http://dx.doi.org/10.6113/JPE.2016.16.6.2173
ISSN(Print): 1598-2092 / ISSN(Online): 2093-4718

Sensorless Scheme for Interior Permanent Magnet Synchronous Motors with a Wide Speed Control Range

Chan-Hee Hong*, Ju Lee*, and Dong-Myung Lee†

*Division of Electrical and Biomedical Engineering, Hanyang University, Seoul, Korea
†School of Electronic and Electrical Engineering, Hongik University, Seoul, Korea

Abstract

Permanent magnet synchronous motors (PMSMs) have higher torque and superior output power per volume than other types of AC motors. They are commonly used for applications that require a large output power and a wide range of speed. For precise control of PMSMs, knowing the accurate position of the rotor is essential, and normally position sensors such as a resolver or an encoder are employed. On the other hand, the position sensors make the driving system expensive and unstable if the attached sensor malfunctions. Therefore, sensorless algorithms are widely researched nowadays, to reduce the cost and cope with sensor failure. This paper proposes a sensorless algorithm that can be applied to a wide range of speed. The proposed method features a robust operation at low–speed as well as high–speed ranges by employing a gain adjustment scheme and intermittent voltage pulse injection method. In the proposed scheme the position estimation gain is tuned by a closed loop manner to have stable operation in tough driving environment. The proposed algorithm is fully verified by various experiments done with a 1 kW outer rotor–type PMSM.

Key words: Back–EMF detection–based sensorless control scheme, Gain adjustment, Permanent magnet synchronous motor drive, Sensorless control, Voltage pulse injection

I. INTRODUCTION

Permanent magnet synchronous motors (PMSMs) can be divided into two categories depending on how the magnets are mounted in the rotor: surface–mounted PMSMs (SPMSMs) and interior PMSMs (IPMSMs). Since PMSMs generate magnetic field with permanent magnets (PMs) in the rotor, there is no heat generation, which results in high power factor and efficiency compared to other types of motors [1]. IPMSMs have an advantage of additional reluctance torque due to the salient rotor. Unlike SPMSMs, IPMSMs have a small air gap so that the magnetic flux density is relatively high and have no scattering problem of a magnet at the high–speed operation. Because of these advantages, IPMSMs are widely used in applications requiring properties of high–density output and are favorable for high–speed operation. For the vector control of PMSMs, knowing the exact rotor position is essential. The rotor position is usually detected through position sensors such as an encoder and a resolver.

In limited applications that do not require high performance of field oriented control, less–expensive Hall–effect sensors have been used occasionally. However, there is the difficulty in obtaining accurate information of the rotor position from using Hall sensors of binary–type [2]. On the other hand, a resolver can offer precise information of the rotor position, but it is configured with several parts and relatively expensive.

The position sensors can increase the cost of driving systems, and a malfunction or failure of the position sensor can cause unstable control operation. In some applications such as a compressor drive, a position sensor cannot be used, hence the sensorless operation is required. Therefore to cope with these problems, sensorless algorithms have been researched widely, and a number of sensorless control schemes have been proposed [2]-[15]. Since permanent magnets are located in the rotor of a PMSM, implementation of sensorless method is relatively easier compared with those of other types of motors, and the application of the sensorless driving of PMSM is gradually increasing these days.

Manuscript received Apr. 23, 2016; accepted Jul. 4, 2016
Recommended for publication by Associate Editor Gaolin Wang.
†Corresponding Author: dmlee@hongik.ac.kr
Tel: +82-2-320-3047, Hongik University
*Div. of Electrical and Biomedical Eng., Hanyang University, Korea

Sensorless position estimation techniques of PMSMs can be classified into two as back–EMF (ElectroMotive Force) estimation–based scheme and rotor position detection by high frequency (HF) signal injection. The back–EMF detection–based scheme estimates the rotor position by manipulating the errors between stator currents in the controller and those from a motor model. Basically, this method employs the discrete current values from motor state equations and sometimes applies complex observer schemes [3], [4]. The precision of the estimated position is highly affected especially at low–speed operation by the accuracy in motor parameters and nonlinearity in inverter output voltage such as dead–time effect [5]. The magnitude of the back–EMF at low–speed range is small, in which the back–EMF based sensorless method is primarily useful at medium–speed or higher [6].

The second method, namely, HF signal injection, detects rotor position by using the saliency of an electric motor [7]-[9]. In general, this scheme determines rotor position through the signal processing of the feed–backed motor currents after applying specific HF signals [10]. The motor currents corresponding to the injected HF voltage signals have the information of the rotor position due to the saturation characteristics of PM or the saliency in the rotor side. A sine or rectangular wave can be used as a carrier wave, and the carrier signals can be superimposed as voltage commands on the stator or the synchronous coordinate axis [10]-[12]. In [13], a position estimation algorithm used an observer system designed on a synchronous coordinate system was presented. Sensorless schemes with HF signal injection exhibit the disadvantages of audible noise and reduction in the output range of the inverter voltage. Comparing these two sensorless algorithm approaches, merits and demerits of each method can be seen apparently. The method using a motor model without imposing HF voltage signals may show an excellent dynamic characteristic thanks to the back–EMF estimation in real–time. On the other hand, the back–EMF scheme gives relatively poor performance of estimation, in which the EMF magnitude is small.

Meanwhile, the methods of detecting the rotor position by injecting HF voltage signals have a merit of finding out the rotor speed at the low–speed even at standstill. However, the HF injection method requires numerous filters to extract HF signals from detected currents and has time delays caused by using complex calculation processes that result in poor dynamic response. Additional HF voltages or currents generate extra power consumption and noise because of the harmonic components of the audio frequency band [14]. In [15], a sensorless drive scheme that used both saliency– and model–based approaches was presented to improve operation at low-speed range.

To attain stable operation within a wide range of speed, this paper adopts the sensorless algorithm presented in [15]. In [15], the relationship between rotor position errors and the response of the motor current corresponding to the applied voltage pulses are derived. However, practical aspect for applying the pulse injection method to the back–EMF based scheme has not been mentioned. These aspects include characteristics based on position estimation gain and the process of initial position detection. Therefore, this paper presents a sensorless algorithm based on the back–EMF observing method that employs voltage pulse injection algorithm, which is executed once in several PWM periods in order to modify the position information from the back–EMF detection method at low–speed operation. In the medium– or high–speed the rotor position is detected based on EMF–estimation method. To get more stable operation, this paper proposes a gain adjustment scheme. Usually the position estimation gain may be determined through a large number of experiments, but the process of tuning the gain is very time consuming and moreover, the tests can not reflect a number of different causes. To show the validity of the proposed scheme, experiments are carried out with a 1 kW PMSM. In addition, an initial position searching out method is explained and experimental result is given. Operations in the starting, transient, and steady state operation with 100 % load are demonstrated to illustrate the efficacy of the proposed algorithm.

II. Sensorless Method Based on Back–EMF Detection

To enhance the understanding of the proposed algorithm, this section briefly describes the sensorless scheme by using back–EMF estimation. The voltage equation of IPMSM in the synchronous dq–coordinate is expressed as (1).

$$\begin{bmatrix} v_d \\ v_q \end{bmatrix} = \begin{bmatrix} r_s + L_d p & -\omega_r L_q \\ \omega_r L_d & r_s + L_q p \end{bmatrix} \begin{bmatrix} i_d \\ i_q \end{bmatrix} + e \begin{bmatrix} 0 \\ 1 \end{bmatrix} \quad (1)$$

where, v_d and v_q are d– and q– axis voltages. i_d and i_q represent d– and q–axis currents. L_d and L_q are d– and q–axis inductances, ω_r denotes the rotor speed, e is the magnitude of EMF, and p represents the differential operator d/dt.

Fig. 1 shows the actual axis (dq–axis), the controller's axis ($\gamma\delta$–axis), and related position information. d–axis is referred to the axis which the actual rotor flux is located in, q–axis is the quadrature axis of dq–axis, and $\gamma\delta$–axis is the estimated synchronous rotating frame, which has the position error as $\Delta\theta$ with respect to the actual axis dq. θ and θ_c are the angular position of actual position and that in controller, respectively. The actual rotor angle θ rotates with the dq–axis, and this axis cannot be detected directly during sensorless operation. All the control operations are manipulated with the variables on the $\gamma\delta$–axis by using the estimated rotor angle θ_c. ω_c denotes the rotational angular velocity.

Since the rotor position in the controller differs from that in actual axis, the EMF–component (e), which should appear only in q–axis, exists in γ– as well as δ–axis with certain portion, and the motor voltage equations in the $\gamma\delta$–axis can be given as (2). The equations rearranged with differential form

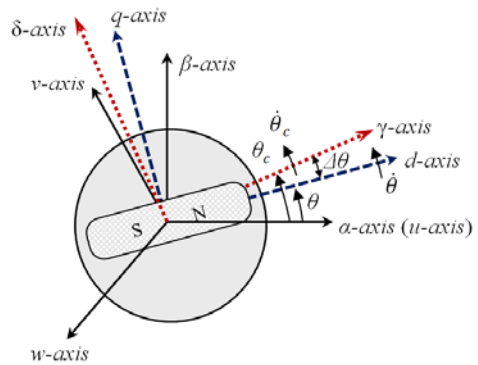

Fig. 1. Stationary and rotating reference frames of the actual axis (dq) and the controller axis ($\gamma\delta$).

of motor currents can be expressed as (3). Subscript c represents the value in the controller.

$$\begin{bmatrix} v_\gamma \\ v_\delta \end{bmatrix} = \begin{bmatrix} r_s + L_d p & -\omega_c L_q \\ \omega_c L_d & r_s + L_q p \end{bmatrix} \begin{bmatrix} i_\gamma \\ i_\delta \end{bmatrix} + e \begin{bmatrix} -sin\Delta\theta \\ cos\Delta\theta \end{bmatrix} \tag{2}$$

$$p\begin{bmatrix} i_\gamma \\ i_\delta \end{bmatrix} = \begin{bmatrix} -r_s / L_d & \omega_c L_q / L_d \\ -\omega_c L_d / L_q & -r_s / L_q \end{bmatrix} \begin{bmatrix} i_\gamma \\ i_\delta \end{bmatrix} + \begin{bmatrix} v_\gamma / L_d \\ v_\delta / L_q \end{bmatrix} + e \begin{bmatrix} sin\Delta\theta / L_d \\ -cos\Delta\theta / L_q \end{bmatrix} \tag{3}$$

Assume that the angle difference between the dq– and $\gamma\delta$–axes is small, and that it exhibits the relation $\Delta\theta \cong 0$, thereby resulting in $sin\Delta\theta \cong 0$ and $\cos\Delta\theta \cong 1$. Through this approximation, (3) in discrete form can be written as (4). n and n+1 represent the value at the current sampling time and the state variable at the next sampling period, respectively. Subscript M denotes the value obtained from the motor model, and T is the sampling period.

$$\begin{bmatrix} \Delta i_\gamma(n+1) \\ \Delta i_\delta(n+1) \end{bmatrix} = \begin{bmatrix} i_\gamma(n+1) - i_{\gamma M}(n+1) \\ i_\delta(n+1) - i_{\delta M}(n+1) \end{bmatrix}$$
$$= \frac{T}{L_d L_q} \begin{bmatrix} L_q \cdot e_c(n) \cdot sin\Delta\theta(n) \\ L_d \cdot \left(e_M(n) - e_c(n) cos\Delta\theta(n)\right) \end{bmatrix} \approx \frac{T}{L_d L_q} \begin{bmatrix} L_q \cdot e_c(n) \cdot \Delta\theta(n) \\ L_d \cdot \left(e_M(n) - e_c(n)\right) \end{bmatrix} \tag{4}$$

In (4), the difference in back–EMF or that in rotor position is proportional to the discrepancy between the measured and estimated γ–axis currents, and that between the δ–axis currents, respectively. By introducing estimation gains k_e and k_θ, the differences corresponding to EMF (e) and position (θ) can be given as (5).

$$\delta e(n) = -k_e \cdot \Delta i_\delta(n), \delta\theta(n) = k_\theta \cdot \Delta i_\gamma(n) \tag{5}$$

The EMF, the rotor position, and the rotor speed can be obtained as (6)–(8) [16]. The sign function in (7) represents 1 for a positive value of ω_c and −1 for a negative ω_c.

$$e_c(n+1) = e_c(n) + \delta e(n) = e_c(n) - k_e \cdot \Delta i_\delta(n) \tag{6}$$

$$\theta_c(n+1) = \theta_c(n) + \frac{T}{K_E} e_c(n+1) + sgn(\omega_c)\delta\theta(n)$$
$$= \theta_c(n) + \frac{T}{K_E} e_c(n+1) + sgn(\omega_c) k_\theta \Delta i_\gamma(n) \tag{7}$$

$$\omega_c(n+1) = \frac{\theta_c(n+1) - \theta_c(n)}{T} \tag{8}$$

III. Proposed Sensorless Scheme

The proposed sensorless algorithm is based on the EMF estimation method. On the other hand, it is well known that the algorithms based on back–EMF observers encounter inaccurate position estimation due to several reasons such as the nonlinearity in inverter system and small EMF magnitude at low–speed [16]. Hence, this paper proposes a position estimation gain adjustment scheme to enhance control performance by reducing the effect of nonlinearity in the inverter system. Then, it uses the sensorless method presented in [15] to achieve stable estimation at low–speed ranges. Meanwhile, [15] does not mention an initial position detection method nor does it present the related experimental results. The authors believe that the method presented in [15] is suitable for correcting or compensating the position value to a certain extent; however, it is not effective for identifying the specific rotor position because accurate current measurement, dead–time compensation, and information of motor parameters, such as stator resistance r_s, are necessary in that scheme; all of these parameters for position calculation are presented in Table I and (9)-(10) shown in the followings. Therefore, in this paper, the initial position detection by comparing the magnitude of the motor currents in response to rotating voltage reference vectors is presented and experimental verification is given.

A. Position Error Compensation in Low-speed Region by Injecting Voltage Pulse Intermittently

Fig. 2 illustrates the block diagram of the proposed sensorless control scheme with an estimation error compensation loop, a gain adjustment scheme, and an initial position detection algorithm. The switch S is operated once in several PWM cycles at a low–speed range, such as every 50 PWM interrupt periods. By using the detected current, which corresponds to a voltage pulse applied on the γ–axis voltage, the compensation position $\Delta\theta$ is calculated and added to θ_c i.e., the operation of the switch S is gradually reduced as long as the motor speed increases. Above the region where the magnitude of the back–EMF is sufficiently large, S is implemented not to operate i.e., voltage pulses are not injected above medium–speed operation. The voltage pulses are injected into only γ–axis to give less influence on the generated motor torque. The $\gamma\delta$–axis current waveform, and voltage pulse are depicted in Fig. 3.

The amounts of position error represented by Δi_γ and Δi_δ those correspond to the applied the voltage pulse of v_γ can be summarized as Table I [15]. F_x and F_y are the evaluation functions as shown in (9), and I in (9) is expressed as (10) [15]. By using the approximate of the tangent function of two evaluation functions, the amount of position error for each region discriminated by sign of F_x and F_y was obtained.

$$F_X = \Delta i_\gamma + \Delta i_\delta - I$$
$$F_Y = \Delta i_\gamma - \Delta i_\delta - I \tag{9}$$

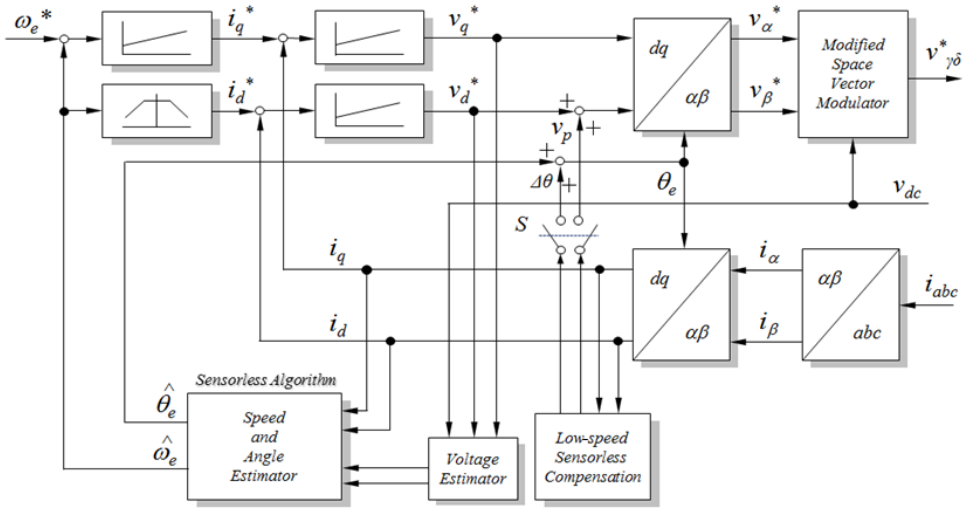

Fig. 2. Overall block diagram of the proposed sensorless scheme with position error compensation, gain adjustment, and initial position detection schemes.

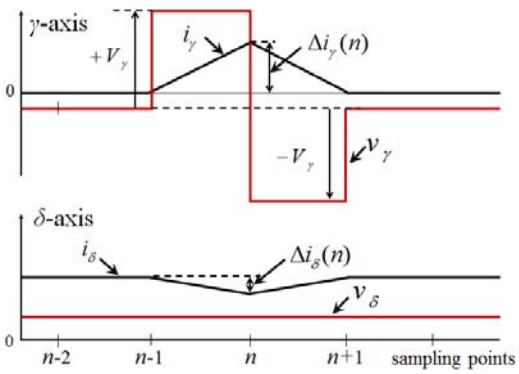

Fig. 3. $\gamma\delta$-axis current waveforms that correspond to voltage pulse v_γ with $\pm V_\gamma$.

TABLE I
COMPENSATION VALUES OF POSITION ERROR FOR EACH REGION

Region of position error	F_x	F_y	Amount of position error ($\Delta\theta$)
$-\frac{7}{8}\pi \sim -\frac{5}{8}\pi$	+	−	$-\frac{\Delta i_r - I}{2\Delta i_\delta} - \frac{3}{4}\pi$
$-\frac{5}{8}\pi \sim -\frac{3}{8}\pi$	−	−	$\frac{\Delta i_\delta}{2(\Delta i_r - I)} - \frac{1}{2}\pi$
$-\frac{3}{8}\pi \sim -\frac{1}{8}\pi$	−	+	$-\frac{\Delta i_r - I}{2\Delta i_\delta} - \frac{1}{4}\pi$
$-\frac{1}{8}\pi \sim +\frac{1}{8}\pi$	+	+	$\frac{\Delta i_\delta}{2(\Delta i_r - I)}$
$+\frac{1}{8}\pi \sim +\frac{3}{8}\pi$	+	−	$-\frac{\Delta i_r - I}{2\Delta i_\delta} + \frac{1}{4}\pi$
$+\frac{3}{8}\pi \sim +\frac{5}{8}\pi$	−	−	$\frac{\Delta i_\delta}{2(\Delta i_r - I)} + \frac{1}{2}\pi$
$+\frac{5}{8}\pi \sim +\frac{7}{8}\pi$	−	+	$-\frac{\Delta i_r - I}{2\Delta i_\delta} + \frac{3}{4}\pi$
$+\frac{7}{8}\pi \sim +\frac{9}{8}\pi$	+	+	$\frac{\Delta i_\delta}{2(\Delta i_r - I)} + \pi$

$$I = \frac{V_\gamma}{r_s}\left\{1 - \frac{1}{2}\left(e^{-\frac{r_s}{L_d}T} + e^{-\frac{r_s}{L_q}T}\right)\right\} \tag{10}$$

B. Adjustment Scheme of Position Estimation Gain k_θ

The gain in (7) can be obtained experimentally by considering the operating environment of the inverter system. However, pilot (or pre–) tests cannot consider all of the factors that affect the performance of position estimation. Determining optimal gain values through a variety of experiments requires considerable time and expense. Moreover, if the estimation gain is defined as a function of operation speed, then the correlations that are generated via load variations and acceleration or deceleration process cannot be reflected.

Hence, this paper proposes a gain k_θ adjustment scheme as depicted in Fig. 4. The gain is adjusted corresponding to the error between Δi_x reference and actual value by utilizing a PI type controller. The amount of the position error according to various k_θ will be shown in the following section. Remarking the experimental results in advance, there is a specific k_θ value resulting in the smallest position error. Smaller or larger than the specific k_θ value, the steady–state position error was increased. The optimal k_θ value depends on many factors such as motor speed, load condition, and the inverter output characteristic. Using the fixed k_θ value can result in unsatisfactory position estimation performance or unstable operation. Hence to cope with a variety of speed, load conditions, and nonlinearity in the system, k_θ varies according to the difference between $\Delta^* i_x$ and Δi_x.

A fixed k_θ with a fairly large value for reducing position error will generate a relatively large ripple in the estimated position, particularly in the steady state, although it provides faster response and generally less position errors. Satisfying the estimation performance in both the transient and steady states with a fixed k_θ value is difficult. In the proposed

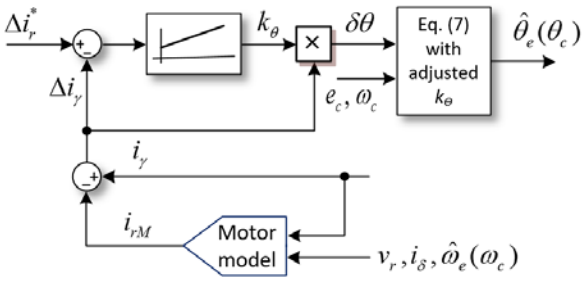

Fig. 4. Block diagram of the proposed k_θ adjustment scheme.

scheme, the k_θ value is automatically adjusted through the action of the PI with respect to the magnitude of Δi_r difference. The proposed gain modification scheme improves dynamic performance in the transient and steady states, as well as prevents ripples in position information in the steady state because of a large k_θ value.

C. Initial Position Detection Scheme

Initial rotor position estimation is one of the major concerns in synchronous motor sensorless control. If a synchronous motor starts with an incorrect initial rotor position, then torque reduction, and in severe cases, reverse rotation, can occur. Especially, in sensorless algorithms if the initially estimated or detected position is not correct, it fails to reduce the position error along with the operation and becomes difficult to expect a stable operation. In this paper, rotor position is obtained by using the saturation characteristic of the magnetic circuit instead of the scheme mentioned in Section III.A. To obtain the initial rotor position more accurately, this position is determined by comparing the motor currents that correspond to the test voltage.

Compared with the linear region of the magnetic circuit, the magnitude of the current in the flux saturation region is relatively large [17]. Therefore, by comparing the detected currents with those that correspond to the injected rotating voltage, the rotor position can be identified relatively easily. When the angle of the applied γ–axis voltage vector approaches the N–pole of the PM in the rotor, the current will be increased because of the magnetic saturation of the PM. On the contrary, away from the N–pole generates a smaller magnitude of the detected γ–axis current. Therefore, the initial rotor position is lying where the voltage vector angle generates the maximum γ–axis current. The magnitude of the applied voltage is chosen big enough to discriminate the magnetic saturation but small enough to not rotate the machine. The experimental will be shown in the next section.

IV. Experimental Verifications

The specifications of the motor used for the experiments are summarized in Table II. The motor is a six–pole and nine–slot IPMSM with an outer rotor type. The rated speed is 1,570 rad/sec. A position sensor resolver was attached only to observe the actual rotor position for investigating the

TABLE II
Specifications of the IPMSM Used for the Experiments

Parameter	Value
DC–link voltage	48 [V_{dc}]
Rated torque	1.9 [Nm]
Rated current	50 [A]
Rated power	1 [kW]
Number of poles	6
Stator resistance	52. 4 [$m\Omega$]
d-axis inductance (L_d)	68.75 [μH]
q-axis inductance (L_q)	104.62 [μH]
EMF coefficient	0.0126 [V/(rad/s)]

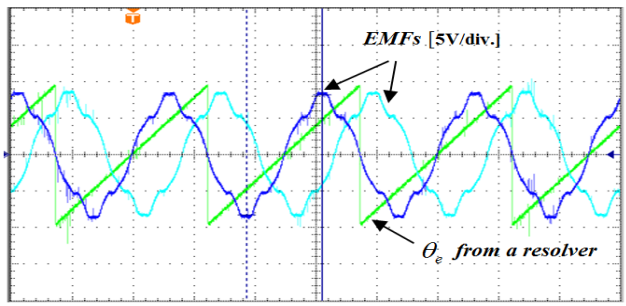

Fig. 5. Measured EMF waveforms and position information obtained using a resolver.

performance of the proposed sensorless algorithm. The control algorithm is implemented via a TI DSP TMS320F28335 with a switching frequency of 10 kHz.

Instead of using Hall CTs, the motor currents were measured by resistors located in the emitter side of power switches to have cost–effect drive system. The IPMSM used in experiments has only 9 slots so that it contains a significant amount of cogging torque can be inferred from Fig. 5 that shows the back–EMF waveforms of the motor. The EMF waveform has large harmonic components. Due to these large harmonics and a small inductance, the current waveform of this motor is not sinusoidal especially at low–speed and/or light load condition.

A. Experimental Results of the k_θ Adjustment Scheme

To observe the effectiveness of the k_θ adaptation scheme, two kinds of experiments without the k_θ adjustment scheme have been carried out first. Fig. 6 shows the experimental waveforms related to position estimation without the k_θ adjustment scheme at a constant speed operation of 100 rad/sec for various k_θ values. As noted in Fig. 6, position errors of 38.7°, 28.2°, 3.2°, and 12.5° are observed for k_θ values of 1, 10, 40, and 80, respectively. At 100 rad/sec constant speed operation, the lowest error occurs for k_θ = 40, and the errors increases when k_θ is smaller or larger than 40. For large k_θ values, such as k_θ = 80, since the amount of position change will increase as can be known from (7), it will generate large ripples in the estimated speed and the motor current.

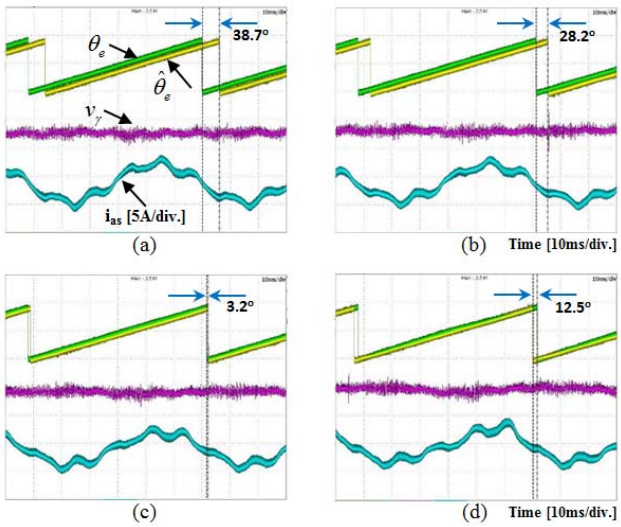

Fig. 6. Position errors for k_θ values of (a) 1, (b) 10, (c) 40, and (d) 80, at 100 rad/sec operation.

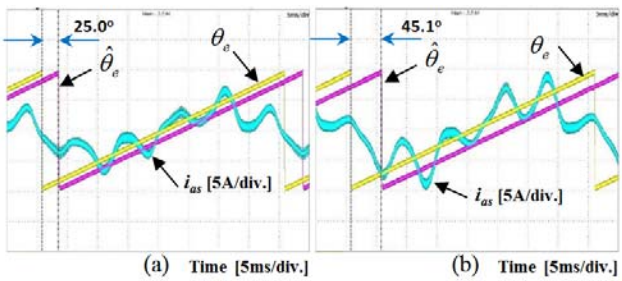

Fig. 7. Position errors corresponding to the relation of (a) $v_{\gamma\delta} = 0.75\ v^*_{dq}$ and (b) $v_{\gamma\delta} = 0.9\ v^*_{dq}$, respectively, at 150 rad/sec operation.

Fig. 7 illustrates the experimental waveforms that are related to the position errors at 150 rad/sec operation with respect to the ratios of v_γ and v_δ, which are the $\gamma\delta$–axis voltage values for the motor model, to the voltage references of controllers v^*_d and v^*_q. In general, the magnitudes of the applied voltages to a motor are less than those of the command voltages due to the voltage drops in power devices and dead–time effects. In Fig. 7(a), v_γ and v_δ are calculated as 75% of v^*_d and v^*_q. In Fig. 7(b), the ratio is selected as 90%. The experiment of Fig. 7 has been conducted to know the tendency of the position error corresponding to the difference between the applied voltage and command one. Figure 7 shows that the position error varies according to the ratio $v_{\gamma\delta}$ to v^*_{dq}, and there is the specific ratio for minimizing the position error. Through the experiments of Fig. 7 with various speed conditions, the relation between v^*_{dq} and $v_{\gamma\delta}$ has been extracted in advance and the derived relationship was applied in selecting $v_{\gamma\delta}$ for the motor model from v^*_{dq} values. In this paper, the ratio has been determined as 68 % at zero speed, an increase of 3 % with respect to 100 rad/sec rise, and an upper limit ratio of 90 %.

Fig. 8 illustrates the experimental waveforms when applying the proposed k_θ adjustment algorithm displayed in Fig. 6. As shown in Fig. 8, the proposed k_θ adjustment scheme exhibits

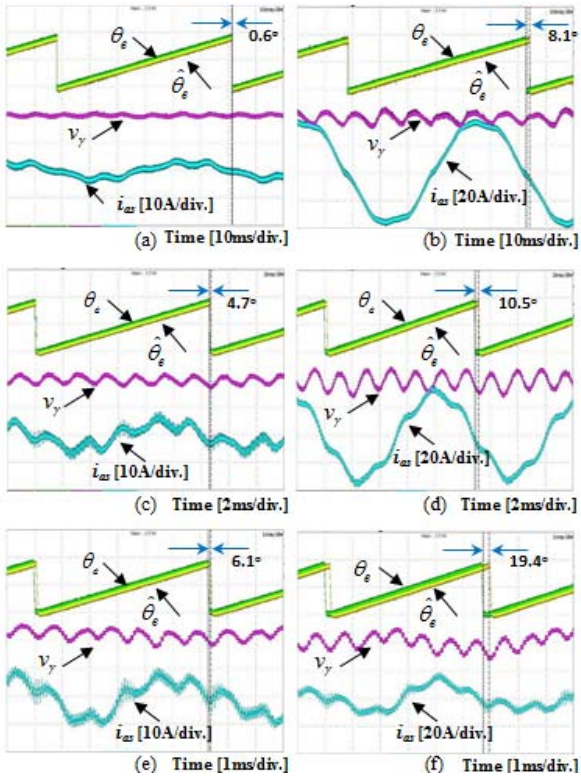

Fig. 8. Experimental waveforms with the proposed k_θ adjustment scheme, which correspond to various speed and load conditions: (a) no load, 100 rad/sec; (b) 1.9 Nm, 100 rad/sec; (c) no load, 500 rad/sec; (d) 2.1 Nm, 500 rad/sec; (e) no load, 1,000 rad/sec; and (f) 1.4 Nm, 1,000 rad/sec.

relatively accurate position estimation for no load as well as heavy load conditions operating at low, medium, and high speeds. A comparison with the error in Fig. 6(c), which shows the lowest error at 100 rad/sec operation, and that in Fig. 8(a), performed under the same load condition, indicates that the proposed scheme demonstrate better performance, with 0.6° position error. In particular, at the low–speed of 100 rad/sec even for the full load operation, the sensorless scheme implemented with the proposed k_θ adjustment method shows the stable position estimation ability as high as 8.1° angle difference.

B. Initial Position Detection

In addition to the previously described k_θ adjustment algorithm, this paper presented two more schemes to improve the performance of the sensorless algorithm. First one was initial position detection scheme and the second algorithm was the compensation of position errors by intermittent voltage pulse injection at low–speed region. Figure 9 shows the experimental results of detecting the initial position located in an arbitrary angle of 123.8 degrees at standstill. The γ–axis voltage of 3 V with 500 Hz rotating angular velocity, which has a voltage level and a frequency that do not rotate the motor, is applied to detect an initial position for the IPMSM with a rated 48 V DC–link voltage. The output voltage vector is

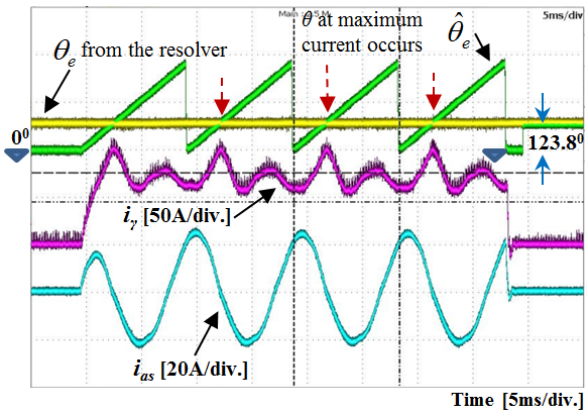

Fig. 9. Experimental waveform of the initial position detection algorithm for the rotor located in an arbitrary position at 123.8°.

rotated four times of the 2π electrical angle. As shown in Fig. 9, the detected motor current reaches its maximum value when the rotor angle matches the angle of the reference voltage vector. Given that current increases from zero amperes at the first rotation, the magnitude is not close to the current value that corresponds to the actual position. Hence, the current values detected from the second to fourth periods were used to obtain the initial rotor position.

C. Position Error Compensation Algorithm Using Intermittent Voltage Pulse Injection at a Low-speed Range

Through the experiments shown in Figs. 9 and 10, reductions in the position errors caused by applying the k_θ adjustment algorithm and waveforms of the initial position detection scheme have been illustrated. However, the aforementioned methods cannot fully reduce degradations of the control performance at low–speed operation because of the small EMF magnitude. The difference between the actual applied voltage and voltage command of the controller significantly affects the accuracy of position estimation. In addition, the uncertainty or variation in the motor parameters in calculating currents using the motor model also has a considerable influence.

Thus, to estimate rotor position at a low–speed range independent of the nonlinearity in the inverter output voltage, the intermittent voltage pulse injection scheme is adopted to supplement the sensorless algorithm. In this sensorless scheme, one voltage pulse is applied in the γ–axis for every 50 PWM periods. Position correction is conducted through Table I using the detected Δi_γ and Δi_δ.

In general, Δi_γ and Δi_δ values are calculated via a complex signal detected process involved in low– and high–pass filtering. The time delay attributed to the use of numerous filtering processes deteriorates the dynamic performance of the controller. Therefore, the Δi_γ and Δi_δ values in this study are obtained by subtracting the sampled values at the current sampling time from the previous values to exclude the use of filters. Figure 10 illustrates the experimental waveforms related

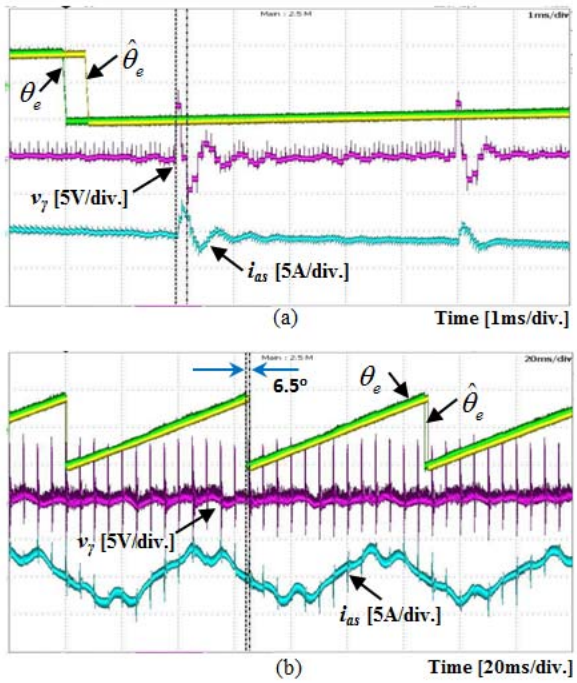

Fig. 10. Experimental waveforms related to the voltage pulse injection method, rotating at 100 rad/sec: (a) position signals, a voltage pulse applied on the γ-axis and the resultant a-phase current and (b) signals shown within a wider time interval.

to the intermittent voltage pulse injection scheme. The actual and estimated positions, γ–axis voltage, and its correspondent a–phase current are shown from top to bottom in the figure. The figure clearly indicates the response of the phase current that corresponds to the voltage pulse.

Fig. 11 illustrates the reduction in position errors via the voltage pulse injection method conducted under 200 rad/sec revolution with 100% full load. The voltage pulse injection algorithm starts at point ①. As shown in Fig. 11, the algorithm significantly reduces position error. The figure shows the electrical angle error of 37.5° before point ①, in which the pulse injection starts. By contrast, the error in angle is reduced to 8.5° via the proposed method. Figure 12 shows the waveforms during operations starting from zero to 100 rad/sec under 100% full load condition. The actual rotor position, γ–axis voltage command, and phase current are displayed from top to bottom in the figure. The proposed method can eliminate the noise problem and the reduction of output voltage utilization ratio that occur in conventional HF injection methods because the scheme applies one voltage pulse once every 50 PWM cycles. As shown in the figure, the position error is already decreased significantly by the proposed scheme before the first revolution. Furthermore, the actual and estimated positions match each other. In addition, the a–phase current exhibits a phase jump whenever position compensation occurs via the voltage pulse injection scheme. It should be noted that in experiments of Fig. 10–12, the scheme of k_θ adjustment were employed.

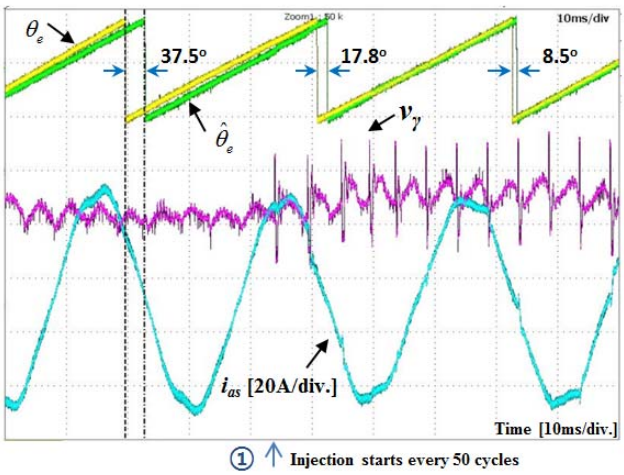

Fig. 11. Reduction of position errors by the voltage pulse injection scheme under 200 rad/sec operation.

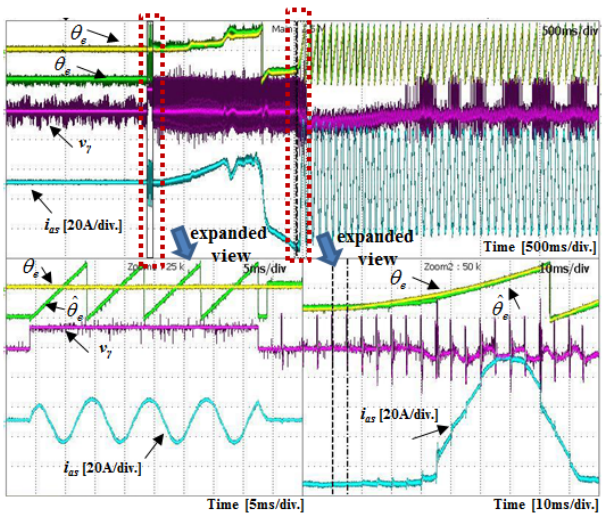

Fig. 12. Sensorless control using the proposed method under full load condition, accelerating from 0 to 100 rad/sec.

V. CONCLUSIONS

This paper proposed a sensorless algorithm for IPMSM. To enhance control performance, the adjustment scheme for position estimation gain was suggested. In particular, this paper adopted the method for compensating position errors through intermittent HF voltage pulse injection at low–speed rotation. To supplement the voltage pulse injection scheme and to achieve stable performance at a wide speed range, the k_θ adjustment scheme was proposed. In addition, the initial position detection scheme was demonstrated with experimental results. The validity of the proposed scheme was confirmed by showing the stable startup with 100% load and the constant speed rotation with full load conditions. To attain a cost–effective driving system, the motor current was detected using shunt resistors, and the use of filtering processes for extracting the HF components of motor currents was excluded.

ACKNOWLEDGMENT

This work was supported by the National Research Foundation of Korea grant funded by the Korean government (Ministry of Science, ICT, and Future Planning, No. NRF–2016R1A2A1A05005392).

This research was supported by the Basic Science Research Program through the National Research Foundation of Korea funded by the Ministry of Science, ICT, and Future Planning (No. NRF–2016R1A2B4011954).

REFERENCES

[1] D. M. Lee, "Position estimator employing Kalman filter for PM motors driven with Binary–type Hall sensors," *J. Elec. Eng. & Tech.*, Vol. 11, No. 4, pp. 931-938, Jul. 2016.

[2] D. M. Lee, D. C. Lim, and H. J. Ahn, "Position linearisation scheme for permanent magnet synchronous motor drive of washing machine using low–resolution hall sensors," *IET Electronics Letters*, Vol. 51, No. 22, pp. 1765-1767, Oct. 2015.

[3] X. Song, J. Fang, B. Han, and S. Zheng, "Adaptive compensation method for high-speed surface PMSM sensorless drives of EMF–based position estimation error," *IEEE Trans. Power Electron.*, Vol. 31, No. 2, pp. 1438-1449, Feb. 2016.

[4] C. X. Chen, Y. X. Xie, and Y. H. Lan, "Backstepping control of speed sensorless permanent magnet synchronous motor based on slide model observer," *Inter. Journal of Automation and Computing*, Vol. 12, No. 2, pp 149-155, Apr. 2015.

[5] Y. Zhao, W. Qiao, and L. Wu, "Dead–time effect analysis and compensation for a sliding-mode position observer–based sensorless IPMSM control System," *IEEE Trans. Ind. Appl.*, Vol. 51, No. 3, pp. 2528-2535, May/Jun. 2015.

[6] M. Seilmeie and B. Piepenbreier, "Sensorless control of PMSM for the whole speed range using two–degree of freedom current control and HF test current injection for low-speed range," *IEEE Trans. Power Electron.*, Vol. 30, No. 8, pp. 4394-4403, Aug. 2015.

[7] Z. Zheng, Y. Li, X. Xiao, and M. Fadel, "Mechanical sensorless control of SPMSM based on HF signal injection and Kalman filter electrical machines and systems," *ICEMS*, pp. 1385-1390, 2008.

[8] O. A. Mohammed, A. A. Khan, A. M. El–Tallawy, A. Nejadpak, and M. J. Roberts, "A wavelet filtering scheme for noise and vibration reduction in high-frequency signal injection-based sensorless control of PMSM at low speed," *IEEE Trans. Energy Convers.*, Vol. 27, No. 2, pp. 250-260, Jun. 2012.

[9] Y. Kano, T. Kosaka, N. Matsui, T. Takahashi, and M. Fujitsuna, "Signal–injection–based sensorless IPM traction drive for wide–torque range operation at low speed," *ECCE*, pp. 2284-2291, 2012.

[10] J. M. Liu and Z. Q. Zhu, "Novel sensorless control strategy with injection of high-frequency pulsating carrier signal into stationary reference frame," *IEEE Trans. Ind. Appl.*, Vol. 50, No. 4, pp. 2574-2583, Jul./Aug. 2014.

[11] C. H. Choi and J. K. Seok, "Pulsating signal injection–based sensorless control of PMSM using injection axis switching scheme without additional offline commissioning test," *IAS Annual Meeting*, pp. 2365-2370,

2007.
[12] A. Piippo, M. Hinkkanen, and J. Luomi, "Sensorless control of PMSM drives using a combination of voltage model and HF signal injection," *IAS Annual Meeting*, pp. 964-970, Vol.2, 2004.
[13] H. Zhu, X. Xiao, and Y. Li, "A simplified high frequency injection method for PMSM sensorless control," *IPEMC*, pp. 401-405, 2009.
[14] W. Limei and G. Qinging, "Principles and implementation of permanent magnet synchronous motor zero–speed sensorless control advanced motion control," *Inter. Workshop on Advanced Motor Control*, pp. 247-250, 2002.
[15] R. Mizutani, T. Takeshita, and N. Matsui, "Current model–based sensorless drives of salient-pole PMSM at low speed and standstill," *IEEE Trans. Ind. Appl.*, Vol. 34, No. 4, pp. 841-846, Jul./Aug. 1998.
[16] N. Matsui, "Sensorless PM Brushless DC motor drives," *IEEE Trans. Ind. Electron.*, Vol. 43, No. 2, pp. 300-308, Apr. 1996.
[17] Y. S. Jeong, R. D. Lorenz, T. M. Jahns, and S. K. Sul, "Initial rotor position estimation of an interior permanent–magnet synchronous machine using carrier–frequency injection methods," *IEEE Trans. Ind. Appl.*, Vol. 41, No. 1, pp. 38-45, Jan./Feb. 2005.

Chan-Hee Hong received his B.S., M.S., and Ph.D. in Electrical Engineering from Hanyang University, Seoul, Korea, in 1991, 1994, and 2015, respectively. From 1993 to 1999, he worked for LG Industrial Systems (currently LS Industrial Systems), Anyang, Korea. From 1999 to 2003, he was employed as a senior engineer by the LG Electronics Home Appliance R&D Center, Seoul, Korea. From 2003 to 2014, he was a chief executive officer of VCTech Co., Ltd., Gunpo, Korea. He has been a senior engineering specialist at Johnson Electric, Hong Kong, since 2014. He was a Senior R&D Manager for DJI, Shenzhen, China in 2012. His current research interests include sensorless synchronous motor control, electrical vehicle traction systems, and autonomous transportation control systems.

Ju Lee received his M.S. degree from Hanyang University, Seoul, South Korea, in 1988, and his Ph.D. from Kyusyu University, Japan in 1997, both in Electrical Engineering. He joined Hanyang University in September, 1997 and is currently a Professor of the Division of Electrical and Biomedical Engineering. His main research interests include electric machinery and its drives, electromagnetic field analysis, new transformation systems such as hybrid electric vehicles (HEV), and high-speed electric trains and standardization. He is a member of the IEEE Industry Applications Society, Magnetics Society, and Power Electronics Society.

Dong-Myung Lee received his B.S. and M.S. in Electrical Engineering from Hanyang University, Seoul, Korea, in 1994 and 1996, respectively, and his Ph.D. in Electrical and Computer Engineering from the Georgia Institute of Technology, Atlanta, Georgia, USA, in 2004. From 1996 to 2000, he worked for LG Electronics Inc., Seoul, Korea. From 2004 to 2007, he was employed as a senior engineer by the Samsung SDI R&D Center, Yongin, Korea. From 2007 to 2008, he was with the Department of Electrical Engineering, Hanyang University, as a research professor. He has been an associate professor at the School of Electronic and Electrical Engineering, Hongik University, Seoul, Korea since 2008. His current research interests include variable speed drives, power quality compensation devices, and power conversion systems for renewable energy sources.